


Stable nanoparticle aggregates/agglomerates of different sizes and the effect of their size on hemolytic cytotoxicity

Justin M. Zook, Robert I. MacCuspie, Laurie E. Locascio, Melissa D. Halter & John T. Elliott


To cite this article: Justin M. Zook, Robert I. MacCuspie, Laurie E. Locascio, Melissa D. Halter & John T. Elliott (2011) Stable nanoparticle aggregates/agglomerates of different sizes and the effect of their size on hemolytic cytotoxicity, *Nanotoxicology*, 5:4, 517-530, DOI: [10.3109/17435390.2010.536615](https://doi.org/10.3109/17435390.2010.536615)



To link to this article: <https://doi.org/10.3109/17435390.2010.536615>

 View supplementary material 

 Published online: 13 Dec 2010.

 Submit your article to this journal 

 Article views: 763

 Citing articles: 109 View citing articles 

Stable nanoparticle aggregates/agglomerates of different sizes and the effect of their size on hemolytic cytotoxicity

JUSTIN M. ZOOK¹, ROBERT I. MacCUSPIE², LAURIE E. LOCASCIO¹,
MELISSA D. HALTER¹, & JOHN T. ELLIOTT¹

¹Biochemical Science Division, and ²Ceramics Division, National Institute of Standards and Technology, Gaithersburg, Maryland, USA

(Received 4 August 2010; accepted 28 October 2010)

Abstract

To study the toxicity of nanoparticles under relevant conditions, it is critical to disperse nanoparticles reproducibly in different agglomeration states in aqueous solutions compatible with cell-based assays. Here, we disperse gold, silver, cerium oxide, and positively-charged polystyrene nanoparticles in cell culture media, using the timing between mixing steps to control agglomerate size in otherwise identical media. These protein-stabilized dispersions are generally stable for at least two days, with mean agglomerate sizes of ~23 nm silver nanoparticles ranging from 43–1400 nm and average relative standard deviations of less than 10%. Mixing rate, timing between mixing steps and nanoparticle concentration are shown to be critical for achieving reproducible dispersions. We characterize the size distributions of agglomerated nanoparticles by further developing dynamic light scattering theory and diffusion limited colloidal aggregation theory. These theories frequently affect the estimated size by a factor of two or more. Finally, we demonstrate the importance of controlling agglomeration by showing that large agglomerates of silver nanoparticles cause significantly less hemolytic toxicity than small agglomerates.

Keywords: Nanotoxicity, silver and gold colloids, hemolysis, engineered nanomaterials

Introduction

Nanoparticle aggregation and the more dynamic process of nanoparticle agglomeration have recently been recognized as significant issues in conducting reproducible toxicity experiments and in interpreting the results (Bihari et al. 2008; Murdock et al. 2008; Jiang et al. 2009; Limbach et al. 2009). The terms aggregation and agglomeration are often used interchangeably, but standards organizations define them distinctly, where aggregation indicates strongly bonded or fused particles and agglomeration indicates more weakly bonded particles (see Supplementary material for full definitions, available online). We use the term agglomeration in this work because our methods likely do not provide enough energy to fuse the particles, even though some aggregates may exist in the original solutions. Many types of nanoparticles (NPs) agglomerate in aqueous biological matrices, such as in phosphate buffered saline and cell culture media, due to the high ionic strength

and neutral pH needed for biological experiments (Chithrani et al. 2006; Bihari et al. 2008; Murdock et al. 2008; Jiang et al. 2009; Kittler et al. 2010; MacCusprie et al. 2010; Tantra et al. 2010; Xie et al. 2010). Other components in biological matrices can also influence the agglomeration process. For example, serum proteins such as albumin will coat many types of NPs and prevent or slow agglomeration (Chithrani et al. 2006; Bihari et al. 2008; Lundqvist et al. 2008; Murdock et al. 2008; Jiang et al. 2009; Kittler et al. 2010; MacCusprie et al. 2010; Tantra et al. 2010; Xie et al. 2010). Depending on the formulation of the biological matrix and the dispersion protocol, identical nanoparticles can agglomerate to different sizes, which significantly complicates the interpretation of cytotoxicity experiments. A few toxicity experiments have compared highly agglomerated NPs dispersed in media without proteins to less agglomerated NPs dispersed with proteins, but it was not possible to determine if the differences in toxicities were due to the presence of

Correspondence: Dr Justin M. Zook, PhD, National Institute of Standards and Technology, Biochemical Science Division, 100 Bureau Drive, MS 8313, Gaithersburg, MD 20899, USA. E-mail: jzook@nist.gov

proteins or the effect of agglomeration (Murdock et al. 2008; Kittler et al. 2010).

Agglomeration is expected to influence NP toxicity by affecting cellular uptake (e.g., Trojan-horse type mechanisms) (Hussain et al. 2006; Limbach et al. 2007; Schrand et al. 2007; Park et al. 2010), affecting the biodistribution of NPs *in vivo* (Greish 2007), decreasing the effective specific surface area to decrease metal ion release (Liu and Hurt 2010) and reactive oxygen species generation (Park et al. 2008; Usenko et al. 2008; Hotze et al. 2010; Kim et al. 2010a), increasing the sedimentation rate (Kato et al. 2010), and changing the shape into a fractal (Weitz and Oliveria 1984; Chithrani et al. 2006; Hotze et al. 2008; Hutter et al. 2010). Therefore, many studies have highlighted the need to explore the effect of agglomeration on the toxicity of NPs (Hussain et al. 2009; Wiesner et al. 2009).

Previous nanotoxicology studies that have controlled agglomeration in solution have generally focused on minimizing agglomeration by methods such as sonication (Murdock et al. 2008) and/or adding proteins or biologically-compatible surfactants (Sager et al. 2007). In most cases, reproducibility of the method used to control agglomerate size is not fully studied. Sonication is a top-down method that starts with agglomerated NPs and breaks them apart. However, sonication has several complications, highlighted in recent NIST-CEINT protocols (Taurozzi et al. 2010a, 2010b, 2010c). For example, it is difficult to reproduce completely the sonication conditions, proteins or NPs may be damaged, and no universal theory exists to predict the size distribution after sonication. Furthermore, it is not clear that minimizing agglomeration by sonication produces the most relevant NP state for toxicity studies.

It is known that many NPs will agglomerate to some extent in biological or environmental solutions before they reach their biological target (Sharma 2009). Therefore, it would be useful to have simple methods to produce dispersions of NPs in different agglomeration states so that the toxicity of the most important size distribution(s) of agglomerates could be studied. Alternatively, if the relevant size distributions are not known, a variety of size distributions of agglomerates could be produced to compare their toxicities.

Separation and fractionation of particles by size may allow investigation of toxicity dependence on agglomeration (Kim et al. 2010a; Okuda-Shimazaki et al. 2010). However, most fractionation techniques are expensive, interact with the sample, or produce different size fractions that may contain different dispersant, seed particle, or nanoparticle concentrations, as well as different nanoparticle compositions in some cases. Furthermore, the simplest fractionation

techniques (e.g., centrifugation or filtration) have generally been used only to compare the toxicity of a sample containing all NP agglomerate sizes to a fraction containing only the smaller sizes, so that interaction between toxicities of large and small agglomerates cannot be excluded. All fractionation techniques require measurement of the NP concentration in each fraction, which is difficult to measure accurately for most NPs. These complications make it difficult to definitively distinguish size effects from other composition-related effects when using fractionation techniques. Another method using electrospray aerosol generation was recently demonstrated to disperse NPs as an aerosol, and initial tests showed that two different carbon nanotube agglomeration states could be produced. However, multiple size distributions of controlled agglomerates were not produced and characterized, and the method requires electrospray instrumentation (Kim et al. 2010b).

To address the need for a simple method to produce NP agglomerates of different sizes that can be easily reproduced in many laboratories, we have developed a bottom-up method that starts with a single well-dispersed NP solution and controllably agglomerates the NPs to different reproducible and stable agglomeration states in an aqueous biological matrix. Depending on the parameters of the method, the mean sizes of the agglomerates range from the primary particle size to larger than 1 μm . We compare several methods of characterizing the agglomeration state, utilize and derive modifications to the analysis of dynamic light scattering data that can affect the diameter by a factor of two or more, and use these results along with colloidal agglomeration theory to estimate the size distribution of the agglomerates. Finally, we use this dispersion method to show that the extent of silver NP agglomeration significantly affects the NP's hemolytic activity. We expect that our method will be applicable to a wide variety of different nanoparticle types that can be agglomerated in aqueous solutions and then stabilized by proteins, and that it will facilitate studying the effect of agglomerate size in many experimental systems that measure biological-nanoparticle interactions, including cellular toxicity, *in vivo* toxicity, bactericidal studies, and cellular imaging experiments (Roca and Haes 2008).

Materials and methods

Materials

Certain commercial equipment, instruments or materials are identified in this report to specify adequately the experimental procedure. Such

identification does not imply recommendation or endorsement by the National Institute of Standards and Technology, nor does it imply that the materials or equipment identified are necessarily the best available for the purpose. Dulbecco's Modified Eagle Medium (DMEM) with 4.5 g/L glucose and sodium pyruvate but without phenol red or L-glutamine was obtained from Mediatech (Manassas, VA, USA). Bovine serum albumin (BSA) was from Sigma Aldrich (St Louis, MO, USA) ($\geq 96\%$, essentially fatty acid free). The antibiotics streptomycin and penicillin were from Invitrogen and were added at 100 $\mu\text{g/mL}$ and 100 U/mL, respectively, to DMEM to reduce bacterial growth. DMEM + 4% BSA by weight was filtered through a 0.2 μm polypropylene filter to remove large protein aggregates that would interfere with the DLS measurements. Citrate-stabilized 30 nm gold nanoparticles (AuNPs) were the standard reference material 8012 from the National Institute of Standards and Technology. Citrate-stabilized silver nanoparticles (~ 23 nm intensity-weighted mean diameter in water by DLS) were produced using a previously described method of reducing an aqueous solution of boiling silver nitrate in the presence of trisodium citrate dihydrate with sodium borohydride obtained from Sigma Aldrich (MacCuspie et al. 2010). The silver nanoparticles were concentrated to ~ 1.1 mg/mL by stirred cell ultrafiltration through a 10,000 Da molecular weight cut off regenerated cellulose filter. For the hemolysis experiments, horse blood anticoagulated with heparin was obtained from Hemostat Laboratories (Dixon, CA, USA). Cerium oxide (CeO_2) NPs with a nominal size of 64 nm specified by the manufacturer were created by Umicore as a 10 mg/mL suspension in 10^{-4} mol/L nitric acid. Aminated polystyrene NPs with a nominal size of 57 nm were created by Bangs Laboratories, Inc. (Fishers, IN, USA) as a 10 mg/mL suspension in water stabilized by a proprietary surfactant.

Nanoparticle dispersion

NP agglomerates are prepared with the following two procedures as depicted in Figure 1. In the first procedure, Figure 1a, a well-dispersed aqueous NP solution is pipetted into a tube containing the cell culture medium (DMEM) with 2% BSA while vortexing to produce the smallest agglomerates (close to the primary particle size). In this case, NPs are stabilized by BSA before they agglomerate to large sizes, with faster mixing resulting in singly dispersed NPs or smaller, more reproducible agglomerates. In the second procedure, Figure 1b, the NP solution is pipetted into DMEM without BSA while vortexing to produce larger agglomerates. In this case, the high ionic strength causes the NPs to agglomerate quickly, and they are allowed to agglomerate for a defined period of time (between 1 s and 10 min in this work) depending on the desired mean agglomerate size and the NP concentration. After the NPs agglomerate to the desired size, BSA is added to coat the NP agglomerates and produce a stable solution of NPs for studying the dependence of toxicity exclusively on agglomeration state.

Specifically, as described in Figure 1a, to obtain the '0 s' agglomerates (singly dispersed or small agglomerates), 0.8 mL DMEM and 1 mL DMEM + 4% BSA were added to a standard 15 mL polystyrene centrifuge tube. Next, 0.2 mL NP solution was added with a pipette to this solution while the vortexer was set to 115 rad/s (1100 rpm) or 199 rad/s (1900 rpm), and it was vortexed for about 30 s after adding the NPs.

To make the 1 s and 5 s agglomerates, as described in Figure 1b, 0.8 mL DMEM was added to a centrifuge tube. The tube was held in place on the vortexer in a foam holder, the vortexer was turned on at 115 rad/s (1100 rpm), and 0.2 mL NP was added followed by 1 mL DMEM + 4% BSA after 1 s or 5 s.

To make the larger agglomerates, as described in Figure 1b, 0.8 mL DMEM was added to a

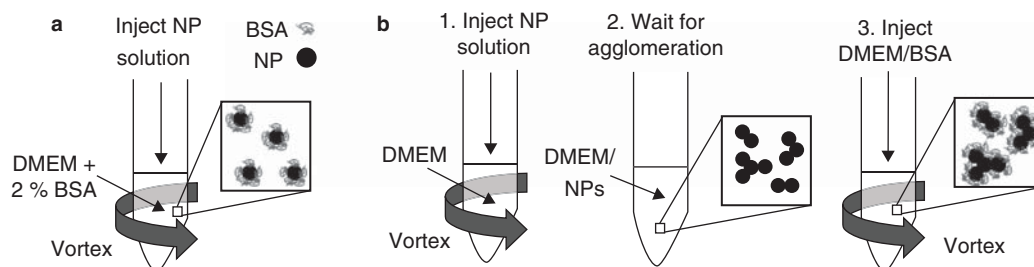


Figure 1. Methods used to produce different agglomeration states of nanoparticles in this work. (a) To minimize agglomeration, a well-dispersed aqueous NP solution was pipetted into the cell culture medium DMEM with 2% BSA while vortexing. (b) To achieve different mean agglomerate sizes, a well-dispersed aqueous NP solution was first pipetted into DMEM without BSA while vortexing. Then, the particles were allowed to agglomerate over time to the desired size before adding 2% BSA to stop agglomeration.

centrifuge tube. The tube was then vortexed while adding 0.2 mL NP solution for about 2 s. After allowing the NPs to agglomerate for the desired time, 1 mL DMEM + 4% BSA was added while vortexing.

For the polystyrene NPs, either the original 10 mg/mL solution of NPs in water was pipetted into DMEM + 2% BSA while vortexing or not mixing, or the 10 mg/mL solution was diluted to 1 mg/mL with water and then this 1 mg/mL solution was pipetted into DMEM + 2% BSA while vortexing. During stability measurements, the samples were kept in the 15 mL centrifuge tubes in a dark 37°C incubator except during the DLS and spectrophotometric measurements.

Spectrophotometry

Spectrophotometric absorbance measurements between 300 nm and 1100 nm were made using a Hewlett Packard 8453 spectrophotometer. The absorbance of the 4.8 µg/mL AuNPs and 6.7 µg/mL AgNPs was measured directly in a 1 cm cuvette, and the background absorbance spectrum of DMEM + 2% BSA was subtracted from all NP spectra. The 110 µg/mL AgNP solution was diluted 20× with deionized water and the absorbance was measured within 1 min.

Dynamic light scattering (DLS)

DLS was performed using a Brookhaven Instruments (Holtsville, NY, USA) ZetaPALS with a 660 nm laser and the detector at 90°. Samples were measured for 100 s. The autocorrelation curve was exported for further analysis in Matlab in order to subtract the scattering signal from BSA.

Because the 4% BSA in DMEM solution was filtered through a 0.2 µm filter, all large agglomerates were removed and the remaining BSA (diluted with DMEM to 2%) had an intensity-weighted mean size of approximately 9 nm by DLS. Simultaneously fitting two exponential decay curves ($A_1 e^{-t/T_1} + A_2 e^{-t/T_2}$) was found to provide a good fit to the autocorrelation curve for BSA using the Matlab curve fitting toolbox, with the fitting parameters obtained as $A_1 = 3.258 \times 10^7$, $T_1 = 29.94$ µs, $A_2 = 3.495 \times 10^6$, and $T_2 = 101$ µs. Since autocorrelation curves are additive, the curve for BSA can theoretically simply be subtracted from the curve for the NP-BSA mixture. However, the absolute intensity of the scattered light varies from run to run on many DLS instruments. Therefore, the weighting of the BSA autocorrelation function was used as a fitting parameter (B_1), in addition to fitting

the part of the curve due to the NPs. The first and second cumulants were fit to the NP part of the curve to provide a better fit to the polydispersity of the NP agglomerates. This resulted in four simultaneous fitting parameters (B_1 , B_2 , T_3 , and β) in Equation 1.

$$B_1(A_1 e^{-t/T_1} + A_2 e^{-t/T_2}) + B_2 e^{-t/T_3 + t^{2/3}} \quad (1)$$

where A and B are scaling parameters that depend on the scattered light intensity, T_1 to T_3 are the first cumulants, and β is the second cumulant. The first cumulant of the NP scattering T_3 was used to calculate the intensity-weighted mean hydrodynamic diameter (d_h) using the well-known Equation 2.

$$T_3 = [k_B T / (3\pi\eta d_h)] q^2 \quad (2)$$

where k_B is Boltzmann's constant, T is the temperature in K, η is the viscosity, $q = (2\pi n/\lambda_0) 2\sin(\theta/2)$ is the scattering vector, n is the medium's index of refraction, λ_0 is the wavelength of light, and θ is the scattering angle.

The effect of BSA scattering on the measured size is most significant for small, unagglomerated, weakly scattering, and/or dilute NPs. For example, 30 nm AuNPs dispersed at 4.8 µg/mL in 2% BSA without agglomeration have a measured diameter of 16.5 ± 1.0 nm with the BSA scattering included, but the diameter is 28.2 ± 1.2 nm after subtracting the scattering due to BSA. However, when the same NPs are allowed to agglomerate even slightly to an average size of 45.9 ± 0.3 nm with BSA scattering included, subtracting BSA scattering only slightly increases the size to 48.4 ± 1.4 nm. Similarly, for the smallest agglomerates of ~23 nm AgNPs dispersed at 6.7 µg/mL directly in DMEM-BSA, the measured diameter is 20.2 ± 2.6 nm with the BSA scattering included, but the diameter is 36.7 ± 1.7 nm after subtracting the scattering due to BSA. For the same NPs dispersed at a higher concentration of 110 µg/mL with slightly larger agglomerates, the measured diameter is 53.5 ± 1.3 nm with the BSA scattering included, and the diameter is 57.7 ± 1.3 nm after subtracting the scattering due to BSA. For even larger agglomerates of AuNPs and AgNPs, the diameter is generally affected less than 5% by the BSA scattering.

Previous work has shown that rotation and vibration of the fractal-shaped agglomerates of NPs significantly influences the signal measured by DLS, so that the measured diameter can be smaller than the actual hydrodynamic diameter by a factor of two or more. This factor was found to be universally dependent on qR , where q is the scattering vector defined above and R is the agglomerate radius (Lin et al. 1990). We fit a function to the published curve, finding

$\exp\{0.867/[1+4.108*(qR)^{-2.1}]\}$ provided a good fit for $qR < 12$. Therefore, all measured effective hydrodynamic diameters were multiplied by this factor. Although this universal curve is not applicable to single particles or very small agglomerates, this factor was close to one for these particles, so it did not significantly affect their diameters. The scattering vector q is a function of the angle at which scattering is measured, so rotation and vibration have a larger effect on scattering at larger angles. For the instrument used in this work, which measures scattering at 90° at a wavelength of 660 nm, the multiplicative factor is 1.04, 1.15, 1.48, 1.97, and 2.26 for measured diameters of 50, 100, 200, 400, and 800 nm, respectively.

Calculating the size distribution from DLCA theory

The compensated intensity-weighted hydrodynamic diameter calculated from DLS can be used to estimate the size distribution of the agglomerates using diffusion-limited colloidal aggregation (DLCA) theory (Lin et al. 1990). DLCA assumes the aggregation/agglomeration kinetics are such that particles permanently stick to each other every time they encounter another particle or clump of agglomerated particles. Adding a high ionic strength solution sufficiently lowers the electrostatic repulsion between citrate-stabilized AuNPs and AgNPs so that their agglomeration is likely to approach DLCA.

When assuming DLCA, the Smoluchowski agglomeration rate equations predict that the particle mass distribution is (Lin et al. 1990):

$$N(M) = \frac{N_0}{M^2} \left(1 - \frac{1}{M}\right)^{M-1} \quad (3)$$

where $N(M)$ is the number of agglomerates consisting of M particles, N_0 is the total number of particles if no agglomeration occurs, and the mean number of particles per cluster $\bar{M} = N_0/N_t$, where N_t is the total number of clusters.

The number of particles in an agglomerate M can be converted into the geometric agglomerate diameter using the equation $d_g = d_p M^{1/d_f}$, where d_p is the diameter of a single particle and d_f is the fractal dimension of the agglomerate, known for DLCA to be approximately 1.86 (Lin et al. 1990). The geometric diameter is directly related to the hydrodynamic diameter by the equation $d_h = 0.93d_g$ (Lin et al. 1990).

The cluster number distribution described by Equation 3 can be converted to the more common

mass-weighted size distribution in several steps. First, \bar{M} can be calculated from the compensated intensity-weighted hydrodynamic diameter calculated from DLS using the numerically determined equation

$$\bar{M} = 0.5 \left(1 + \left[\frac{d_h}{1.1d_p} \right]^{d_f} \right) \quad (4)$$

Next, the right side of Equation 3 is multiplied by $\left(\frac{M^{2-\frac{1}{d_f}}}{\bar{M}} \right)$ to give the proper weighting, which includes contributions due to the increasing mass of agglomerates (M^1) and due to the change in the x-axis from number of particles per agglomerate to the hydrodynamic diameter

$$\frac{dM}{dd_h} \sim d_h^{d_f-1} \sim M^{1-\frac{1}{d_f}} \quad (5)$$

Finally, the distribution is normalized to give an area under the curve equal to one.

AFM methods and image analysis

AFM Images were collected on a Dimension 3100 with a Nanoscope V controller (Bruker AXS, Santa Barbara, CA, USA) in intermittent contact or 'tapping' mode using AFM tips with nominal spring constants of 7 N/m (NanoAndMore, Lady Island, SC, USA). Methodology followed the Nanotechnology Characterization Laboratory Assay Cascade (NIST-NCL PCC-6 'Size Measurement of Nanoparticles Using Atomic Force Microscopy'). Sample prep was carried out in a BSL-2 cabinet. Approximately 20 μ L of solution was incubated for 8 min (110 μ g/mL AgNPs) or 30 min (6.7 μ g/mL AgNPs) on aminated substrates (either polished Si wafer pieces functionalized with 3-aminopropyltrimethylethoxysilane, or freshly cleaved mica discs functionalized with 0.01% poly-L-lysine) before rinsing with filtered deionized water and drying with filtered compressed air.

The 'Analyze Particles' method in ImageJ (<http://rsbweb.nih.gov/ij/>) was used to count semi-automatically the total number of particles in ten $20 \times 20 \mu$ m images of each sample. The images were first converted to black and white by setting the threshold at a level (65 out of 255) that included particles without including noise. The threshold was kept identical for all images to maintain consistency. After the images were converted to black and white, the 'Analyze Particles' method in ImageJ was used to count the particles.

Hemolysis

The hemolysis experiments were based on the ASTM protocol 'E 2524 – 08: Standard Test Method for Analysis of Hemolytic Properties of Nanoparticles', modified to produce multiple agglomerate sizes and maintain NP stability by using the dispersion protocol developed in this paper. Instead of diluting the NP solution with Dulbecco's phosphate buffered saline as described in the protocol, 40 μ L of heparinized horse blood (diluted 4.5 \times with DMEM + 2% BSA) was added directly to 360 μ L of AgNPs dispersed at different agglomerate sizes in DMEM + 2% BSA. Dilution series of AgNPs were created by combining the appropriate amounts of DMEM + 2% BSA with 110 μ g/mL AgNPs dispersed in DMEM + 2% BSA. As a control, the blood was added to DMEM + 2% BSA without AgNPs. The dispersed AgNPs were stored at room temperature at 110 μ g/mL for 3 h prior to incubation with blood. Then the AgNPs were incubated with the blood for 3 h at 37°C while continuously rotating the centrifuge tubes to avoid sedimentation of blood cells or NP agglomerates. After centrifuging at 800 g to remove the intact red blood cells, the supernatant was centrifuged at 8000 g to remove the agglomerated AgNPs, which also absorbed at 540 nm. The absorbance of the supernatant of each AgNP without blood was also measured after centrifugation, and the absorbance corresponded to <0.5% hemolysis, so the AgNPs did not contribute significantly to the absorbance after centrifugation.

Results

Gold nanoparticle agglomerates

DLS and absorbance measurements were used to characterize the size and stability of 30 nm AuNPs in different agglomeration states prepared using the method in Figure 1. Figure 2 shows the size and absorbance of AuNPs dispersed at several different agglomerate sizes, with average relative standard deviations for size and absorbance of 5% and 3%, respectively, for three replicated dispersions. The agglomeration times ranged from 0 s (i.e., no agglomeration time) to 10 min to achieve mean diameters ranging from 29–324 nm. Figure 2a shows that after formation of the NP agglomerates, the sizes are relatively stable for two days after dispersion in DMEM + 2% BSA, with the size increasing over two days by between 5% and 30%. In contrast, if NPs were added to cell culture media without protein for toxicity experiments, the NPs would quickly agglomerate from their original size of 30 nm to

hundreds of nanometers within minutes. For the same NP dispersions as Figure 2a, Figure 2b shows the absorbance spectra due to localized surface plasmon resonance (SPR), with the peak at 526 nm corresponding to the resonance of a single particle and the peak at longer wavelengths corresponding to the SPR coupling between multiple particles (Link et al. 1999).

Agglomerate size distribution

Since agglomerates are never completely monodisperse (i.e., all the same size), it is important to quantitatively calculate the size distributions in order to determine the relationship between agglomerate size and toxicity. For our agglomeration method, DLCA theory can be used to calculate the theoretical size distributions using the mean size derived from the DLS measurements. To obtain accurate size distributions, in many cases it is important that the DLS measurements are compensated either for BSA scattering or for vibration and rotation of large agglomerates, as described in materials and methods. Subtracting the signal from scattering due to BSA increases the calculated size by a factor of 1.8 for the 30 nm AuNPs dispersed in BSA (i.e., '0 s' in Figure 2). Accounting for vibration and rotation increases the calculated size of the largest AuNP agglomerates by a factor of 1.6. (It also increases the calculated size of the largest AgNP agglomerates shown below by a factor of 2.2.) After compensating for BSA scattering, vibration, and rotation, the theoretical size distributions for each initial agglomerate size of AuNPs are shown in Figure 3. As the agglomeration time increases, the size distribution broadens and shifts to larger sizes. It should also be noted that if the agglomeration is not completely diffusion-limited, the size distributions will be broader and contain greater numbers of smaller agglomerates with a few much larger agglomerates, so that more complex agglomeration theories are needed if the agglomeration occurs more slowly. In this work, the high ionic strength of DMEM produces agglomeration that is expected to be close to diffusion-limited (reflected by the fast increase in agglomerate size). Figure 3 demonstrates the important fact that the size distributions of the agglomerates overlap. However, by estimating the size distribution of each sample of agglomerated NPs, deconvolution of the agglomerated size effect on toxicity is still possible.

Silver nanoparticle agglomerates

AgNPs with a mean size of 23 nm were also studied. In these experiments, we evaluated both

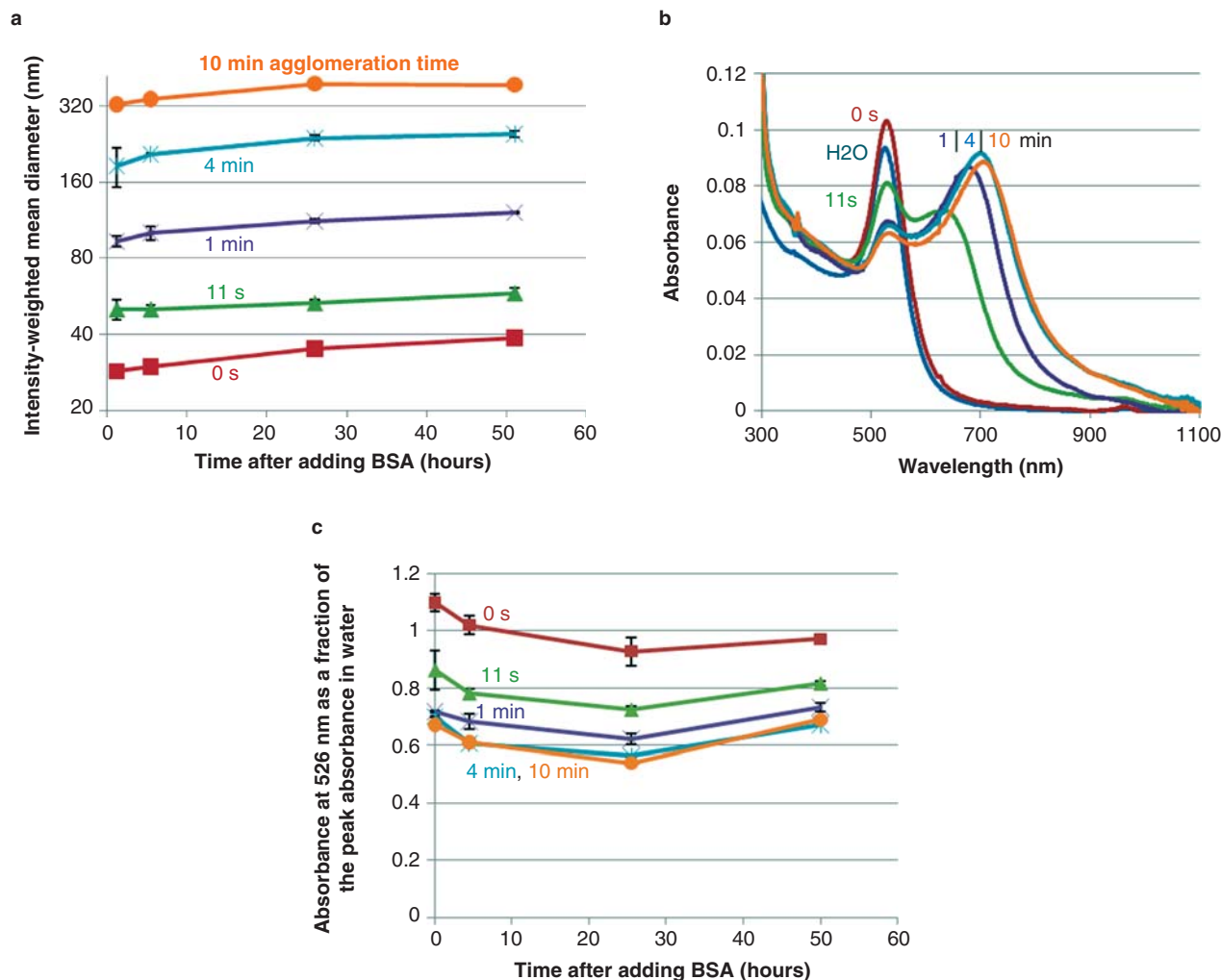


Figure 2. Stability of agglomerates of 30 nm AuNPs over two days at 37°C dispersed at 4.8 $\mu\text{g/mL}$ in DMEM + 2% BSA at five different mean agglomerate sizes. For all graphs, the times labeled inside the Figures correspond to the times between adding the NPs to DMEM and adding BSA to stop the agglomeration process. The x-axes in (a) and (c) are the incubation times after adding BSA. The AuNPs were added to the media while vortexing rapidly at 1900 rpm. (a) The intensity-weighted mean agglomerate size increases by between 5% and 30% over 50 h, calculated from DLS measurements compensated for vibration and rotation of agglomerates. (b) Absorbance spectra of AuNP dispersions in water and in DMEM + 2% BSA measured 5 min after BSA is added (after subtracting background absorbance of DMEM + 2% BSA), with peaks corresponding to the localized SPR excitation across a single particle (at 526 nm) and corresponding to coupled localized SPR excitations between particles (at 650 nm to 750 nm). Spectra after 1 and 2 days are included in Figure S1, available online, in the supporting information. (c) Changes over time of the peak absorbance (at 526 nm) as a fraction of the peak absorbance of the same concentration of non-agglomerated AuNPs dispersed in water. Error bars represent one standard deviation for three replicate samples, and error bars that are not visible are smaller than the data points.

high (110 $\mu\text{g/mL}$) and low (6.7 $\mu\text{g/mL}$) concentrations of NP dispersions to compare their agglomeration and stability. Figure 4a shows that at the high concentration (110 $\mu\text{g/mL}$), the agglomerate sizes were relatively stable in DMEM + 2% BSA, varying by less than 15% over three days regardless of the initial agglomerate size (corresponding to the time before BSA was added). In contrast, the size changed drastically over three days for the lower concentration of NPs (6.7 $\mu\text{g/mL}$), which is discussed further below. Agglomeration occurs very quickly in DMEM at 110 $\mu\text{g/mL}$, so the agglomeration times are much

shorter at this high concentration compared to the low concentration of AuNPs (4.8 $\mu\text{g/mL}$). When dispersing the AgNPs at a high concentration directly in DMEM + 2% BSA, the mixing speed while adding the aqueous AgNP solution was also shown to affect the mean agglomerate size and reproducibility. Figure 4a shows that faster mixing (i.e., higher vortexing speed) produces more reproducible and smaller agglomerate sizes closer to the primary particle size. When dispersing AgNPs at 6.7 $\mu\text{g/mL}$, it is easier to disperse the particles at close to the primary particle size, suggesting that at this concentration

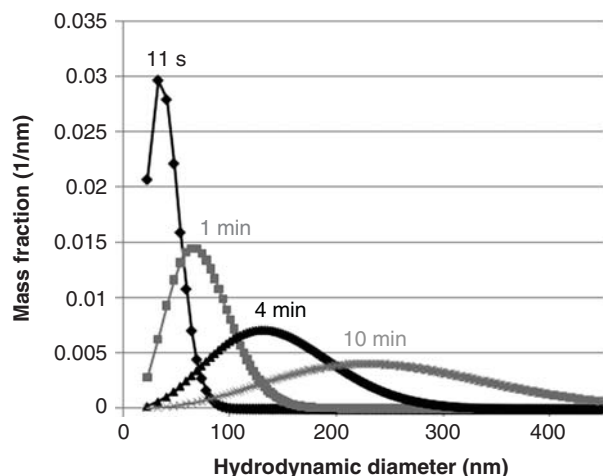
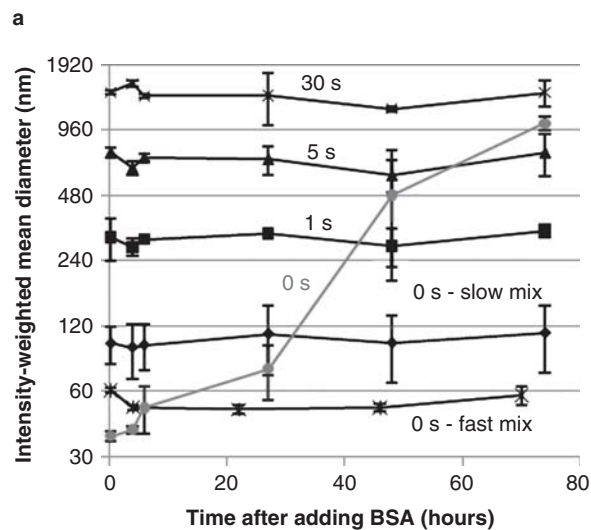


Figure 3. Theoretical mass-weighted size distributions of same AuNP agglomerates in Figure 2 that were allowed to agglomerate in DMEM for 11 s (black diamonds), 1 min (gray squares), 4 min (black triangles), and 10 min (gray crosses) before adding BSA. Each size distribution curve is labeled with its agglomeration time on the graph. The size distributions were calculated from the mean size measured by DLS 5 min after dispersion, compensating for vibration and rotation and BSA scattering and assuming irreversible diffusion-limited colloidal aggregation. Each point represents a single agglomerate size (i.e., for agglomerates in which the number of 30 nm AuNPs is 1, 2, 3, etc.).



the agglomeration rate is probably slow compared to the BSA adsorption rate. The average relative standard deviations for size and absorbance were 9% and 8%, respectively, for three replicated dispersions, excluding the dispersions during slow mixing and the times after 4 h for 6.7 $\mu\text{g/mL}$ AgNPs.

The absorbance spectra of AgNPs (Supplementary Figure S2, available online) are very similar to the AuNP spectra except that the localized SPR occurs at shorter wavelengths. Figure 4b shows changes of the absorbance peak at 397 nm, which corresponds to the peak localized SPR absorbance of AgNPs without coupling between nearby particles.

We used AFM to help interpret the DLS and absorbance measurements of AgNPs. One unresolved question about the absorbance spectra is whether the peak height at 397 nm can be quantitatively correlated to the singly dispersed AgNP concentration when agglomerates are also present. Although it is difficult to get quantitative measurements of the particle size distribution using AFM, we generally observed more large agglomerates as the agglomeration time increased. In Figure 5, we depict the number of agglomerates on the AFM substrate as a semi-quantitative measure of agglomeration, with the number of agglomerates decreasing as agglomeration time

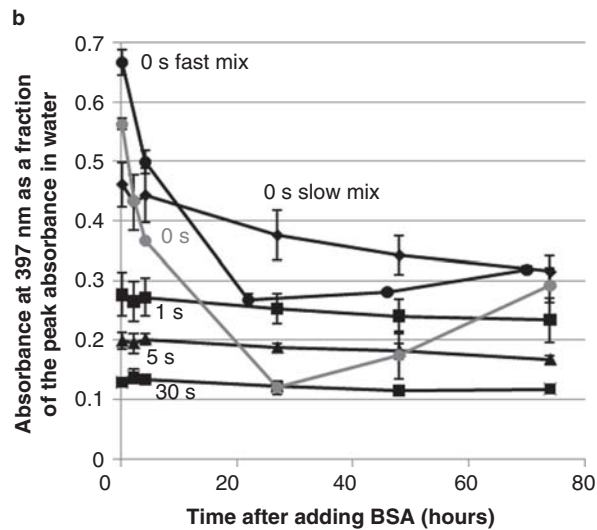


Figure 4. Stability of agglomerates of 23 nm AgNP in DMEM + 2% BSA over three days at 37°C dispersed at 110 $\mu\text{g/mL}$ (black) at four different initial agglomerate sizes, corresponding to allowing NPs to agglomerate in DMEM for approximately 0 s, 1 s, 5 s, or 30 s before adding DMEM-BSA. For the 0 s dispersions, the AgNPs were added to DMEM + 2% BSA while vortexing slowly (at 1100 rpm) or quickly (at 1900 rpm). In addition, the stability of AgNP agglomerates at 6.7 $\mu\text{g/mL}$ (gray), with BSA added at 0 s while vortexing at 1900 rpm, is shown. (a) Stability of the agglomerate size over time, as measured by the compensated intensity-weighted mean agglomerate size calculated from DLS. (b) Stability of the peak absorbance (at 397 nm) of dispersed AgNPs as a fraction of the peak absorbance (at 390 nm) of the same concentration of non-agglomerated AgNPs dispersed in water. For both graphs, the times labeled inside the Figures correspond to the agglomeration times between adding the NPs to DMEM and adding BSA to stop the agglomeration process. The x-axes in both graphs are the incubation times after adding BSA. Error bars represent one standard deviation of three samples.

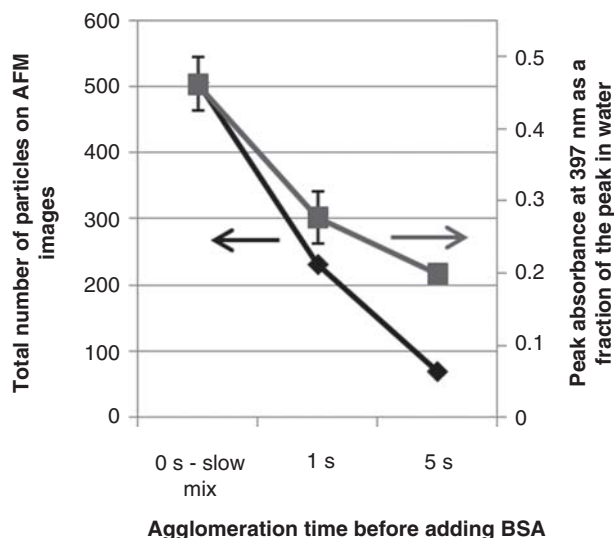


Figure 5. Total number of agglomerates (black diamonds) on ten randomly selected $20\ \mu\text{m} \times 20\ \mu\text{m}$ AFM sections for three agglomeration states of AgNPs at $110\ \mu\text{g/mL}$, showing the decrease in the number of agglomerates as agglomeration time increases, as expected. The agglomerate count on the AFM substrate decreases more than the absorbance at $397\ \text{nm}$ (gray squares) decreases, suggesting that the absorbance at $397\ \text{nm}$ is not only caused by single particles but may also be caused by some particles that are a part of agglomerates. Representative AFM images are in Figure S4 in the Supplementary material, available online.

increased. Since the proportional decrease of agglomerates in AFM is greater than the proportional decrease in the absorbance at $397\ \text{nm}$, the absorbance at $397\ \text{nm}$ may not be a direct measure of the number of singly dispersed particles in the solution if agglomerates are present. It is possible that particles in small agglomerates and on the outside edge of agglomerates contribute to the absorbance at $397\ \text{nm}$ in addition to single particles.

Cerium oxide agglomerates

Cerium oxide nanoparticles with a nominal size of $64\ \text{nm}$ were found to be aggregated/agglomerated even in pH 4 nitric acid solutions to about $250\ \text{nm}$ (DLS mean diameter compensated for vibration and rotation), and sonication only caused further aggregation. However, as shown in Figure 6 in gray, we were still able to control their agglomeration to achieve mean diameters ranging from $260\text{--}1700\ \text{nm}$. The mean sizes of the NPs dispersed at the high concentration of $1\ \text{mg/mL}$ changed by less than 20% over 48 h.

Positively-charged polystyrene agglomerates

Positively-charged amine-modified polystyrene NPs with a nominal size of $57\ \text{nm}$ were dispersed at $1\ \text{mg/mL}$ and $0.1\ \text{mg/mL}$ using several different protocols to demonstrate the importance of the precise dilution protocol. Possibly because the polystyrene NP solution contains an unknown dispersant, the NPs did not

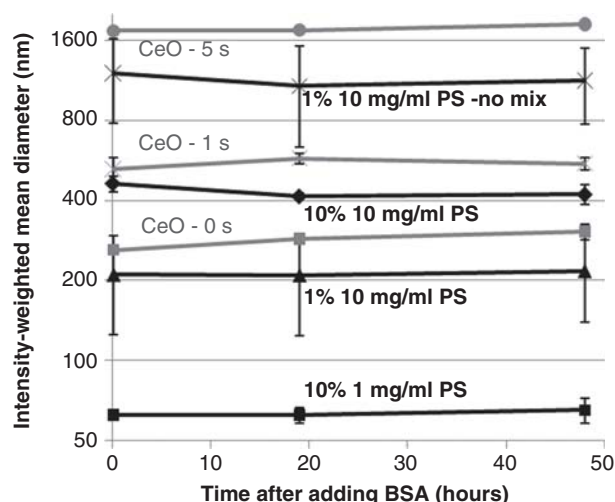


Figure 6. Controlled agglomeration and stability of $\sim 64\ \text{nm}$ cerium oxide NPs (gray) and $\sim 57\ \text{nm}$ positively-charged amine-modified polystyrene NPs (black) in DMEM + 2% BSA over two days at 37°C . The cerium oxide NPs were dispersed at $1\ \text{mg/mL}$, and the times labeled inside the figures correspond to the agglomeration times between adding the NPs to DMEM and adding BSA to stop the agglomeration process. The agglomeration of the polystyrene NPs depended on the concentrations of NPs both in the injected water solution and in the final dispersed solution. Either 1% or 10% of a $1\ \text{mg/mL}$ or $10\ \text{mg/mL}$ solution of polystyrene NPs dispersed in water was pipetted into a solution containing DMEM + 2% BSA, demonstrating that the agglomeration state can depend on the precise order in which dilution series are carried out. In addition, if the NP solution was pipetted into a stagnant DMEM-BSA solution without vortexing, then the sizes were very large and irreproducible. The x-axes in both graphs are the incubation times after adding BSA. Error bars represent one standard deviation of three samples.

agglomerate to large sizes greater than a few hundred nanometers even in DMEM without proteins. However, they still agglomerated to a couple hundred nanometers, and agglomeration depended on the dilution protocol, as shown in Figure 6 in black. When a 10 mg/mL NP solution was dispersed at 1 mg/mL (10%) in DMEM-BSA while vortexing, the mean agglomerate size was 460 nm. When NPs were dispersed at 0.1 mg/mL, the mean agglomerate size depended on the concentration of NPs in the water solution that was injected. If the 10 mg/mL NP solution was pipetted directly into DMEM-BSA at 1% while vortexing, the mean sizes obtained were 210 ± 85 nm. If the 10 mg/mL NP solution was pipetted into a stagnant solution without vortexing until after pipetting, the mean sizes were much larger and irreproducible, with mean sizes ranging from 750–1600 nm for different samples. However, if the NP solution was first diluted to 1 mg/mL with water, and then the 1 mg/mL solution was pipetted into DMEM-BSA at 10% while vortexing, the mean size was 62 ± 2 nm, close to the primary particle size and very reproducible. Therefore, polystyrene NP agglomeration can still be controlled to some extent by varying the concentration of the injected NP solution, although the agglomerates probably do not follow diffusion-limited aggregation theory.

Dependence of hemolysis on the agglomeration of AgNPs

Figure 7 shows the dependence of hemolysis on the agglomeration state and concentration of AgNPs, with the half-maximal effective concentration (EC_{50}) value increasing for increasing agglomerate size. The highest concentration of AgNPs (110 $\mu\text{g/mL}$) causes almost complete hemolysis for all samples independent of agglomerate size. However, for 13.8–55 $\mu\text{g/mL}$ AgNP concentrations, agglomerates of AgNPs with compensated intensity-weighted mean DLS sizes of 1100 nm and 1400 nm cause significantly less hemolysis than smaller agglomerates ($p < 0.01$).

Discussion

The methods depicted in Figure 1 are able to create solutions with tuned sizes of nanoparticle agglomerates of four different types of nanoparticles (gold, silver, cerium oxide, and amine-modified polystyrene). Because the agglomerates are formed from a well-dispersed starting solution, aggregation theory can be used to estimate the agglomerate size distributions from DLS without using complex or time-consuming size distribution measurement techniques, as shown in Figure 2. Although the

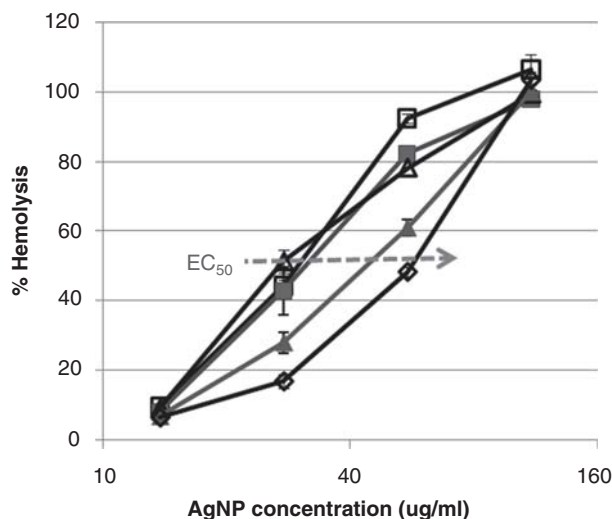


Figure 7. Percentage hemolysis caused by increasing concentrations of 23 nm AgNPs dispersed in DMEM + 2% BSA at five mean agglomerate sizes: 43 nm (black open squares), 190 nm (gray filled squares), 490 nm (black open triangles), 1100 nm (gray filled triangles), and 1400 nm (black open diamonds). The five different compensated intensity-weighted mean agglomerate sizes (calculated from DLS) were created by adding BSA at 0 s, 1 s, 5 s, 30 s, and 120 s after adding the AgNPs to DMEM. The EC_{50} was larger for the two largest mean agglomerate sizes, and at 13.8 $\mu\text{g/mL}$, 27.5 $\mu\text{g/mL}$, and 55 $\mu\text{g/mL}$, the hemolysis caused by the two largest mean agglomerate sizes was significantly less than the hemolysis caused by the smallest agglomerate size ($p < 0.01$). Error bars correspond to the standard deviation of measurements on three blood samples. An alternative representation of the data plotting % hemolysis vs. mean agglomerate size is in Figure S5 in the Supplementary material, available online.

agglomerate size distributions will generally overlap to some extent, deconvolution of the effect of agglomerate size on toxicity is possible since the size distributions can be estimated. By using 2% BSA to coat and sterically stabilize the NPs or NP agglomerates, the sizes change by less than 30% over 2–3 days. This stability time is sufficient for most cytotoxicity experiments, so it is expected that this method can be used to study the effect of agglomeration in most NP cytotoxicity experiments. When comparing the toxicity of different primary sizes of particles, it is usually difficult to distinguish effects of size from the effects of differing concentrations of both the NPs and other contaminants in the samples. With this agglomeration method, different sizes of agglomerates of a single NP type can be created, so that mass concentrations of the NPs and other contaminants will not vary from sample to sample.

Characterization of agglomeration

Characterizing the agglomeration of NPs in a biological matrix is difficult due to interference from biological

components and because light scattering from a mixture of different sizes of fractal-shaped agglomerates is complex. Dynamic light scattering (DLS) is the most common simple and versatile technique for measuring agglomeration in aqueous solutions (Murdock et al. 2008) and works well for estimating the size of the largest agglomerates, but it has several complications, including the following: (i) The effects of vibration and rotation of the agglomerates are usually neglected, which frequently decrease the measured size by a factor of 2 or more (Lin et al. 1990); (ii) measurements are subject to interference from scattering by proteins in the solution; (iii) it is difficult to measure smaller particles that may exist in the presence of large agglomerates because the scattered light intensity is much greater for large agglomerates compared to small particles; and (iv) size distributions are difficult to estimate because many different size distributions can produce practically identical DLS measurements. Electron microscopy and atomic force microscopy (AFM) are also commonly used, but since the samples are usually dried, it is difficult to distinguish agglomeration in the aqueous phase from agglomeration caused by drying without careful sample preparation procedures. For certain NPs, such as the gold and silver NPs used in this paper, UV/visible spectrophotometry can be used to help characterize agglomeration since the localized SPR bands change upon agglomeration (Elghanian et al. 1997; Duan et al. 2009).

In this work, we characterize agglomeration with DLS, absorbance, and AFM in combination with diffusion-limited colloidal aggregation (DLCA) theory to estimate the size distribution. We use DLS to estimate the intensity-weighted mean diameter, compensating for vibration and rotation of the agglomerates using previously published data, which decreases the measured size by a factor greater than two for large agglomerates (Lin et al. 1990). Instead of adding 10% serum (or about 0.6% total protein) to the cell culture medium to coat and stabilize the NPs, we add 2% bovine serum albumin (BSA). BSA was used because albumin is the predominant protein in serum (>50% of the total protein) and is sufficiently small to allow size measurements of the NPs using DLS. We filter the BSA to avoid scattering from large BSA agglomerates, and we develop a method to subtract the BSA scattering signal from the total scattering to obtain better estimates of the NP size. The materials and methods section includes the methods used to compensate for vibration and rotation of agglomerates and for BSA scattering, as well as a discussion of when they significantly affect the measured size. To overcome the limitations of DLS in measuring the size distributions of polydisperse samples, our bottom-up method of agglomerate formation allows the

mean diameter measured by DLS compensated for vibration and rotation to be used with DLCA theory to estimate the size distribution of agglomerates, which is described in more detail in materials and methods. The absorbance spectrum due to the localized SPR bands is used to estimate qualitatively the degree of agglomeration and the concentration decrease due to dissolution of the particles. Finally, AFM of selected samples is used to corroborate DLS and absorbance measurements by measuring the size and number of individual particles. To avoid additional agglomerate formation while drying the NP solution on the AFM substrate, positively-charged aminated substrates were employed so that the negatively-charged BSA-coated NPs and agglomerates would electrostatically adsorb to the surface, and the surface was then rinsed with DI water before drying with a nitrogen stream.

Nanoparticle agglomeration and stability

For all types of NPs, the mean agglomerate size measured by DLS is generally stable, changing by less than 20% over 2–3 days. In addition, localized SPR phenomena can be used to characterize gold and silver NP agglomeration. For both NPs, it is clear that the first peak decreases and the second peak increases and red-shifts as agglomeration increases, indicating increasing coupling of SPR between particles as expected. However, after protein is added, the shape of the absorbance spectra changes very little, reflecting minimal changes in agglomeration. In addition, decreases in the absorbance spectra can indicate metal ion dissolution or small amounts of agglomeration. For AuNPs, Figure 2c demonstrates that the absorbance at the first peak changes over two days, showing a decrease of 15–20% over the first day, possibly corresponding to small increases in agglomeration. The reason for the absorbance increase after the first day is unclear, but it may be due to scattering by large particulate contaminants such as biological organisms or dust, since the entire baseline from 300–1100 nm increases with larger increases at lower wavelengths (see full spectra after 1 and 2 days in Figure S1 in the Supplementary material, available online).

AgNPs are known to dissolve in aqueous solutions over time (Liu and Hurt 2010), and the high concentration of chloride ions and other complexing agents present in physiological solutions facilitates dissolution by forming AgCl and other silver complexes. At 6.7 $\mu\text{g/mL}$ AgNPs, the absorbance at 397 nm rapidly decreases over 24 h without a large increase in absorbance at longer wavelengths (see Figure 4b and Figure S2, available online). Therefore, we hypothesize that the AgNPs are dissolving

significantly over this period of time, and the Ag^+ ions are sequestered by binding to chloride, BSA, and possibly other cell culture media components such as cysteine and carbonate. After 2–3 days the absorbance increases again, but because there is no clear SPR peak (see Figure S2b–d, available online), we hypothesize that this effect is due to light scattering from AgCl or other non- Ag^0 particles. This hypothesis is supported by the increase in particle size measured by DLS for 6.7 $\mu\text{g/mL}$ AgNPs and by AFM images taken of this sample after two days that still had a significant number of larger particles on the substrate (see Figure S3, available online). For 110 $\mu\text{g/mL}$ AgNPs, the absorbance at 397 nm does not decrease as quickly compared to the 6.7 $\mu\text{g/mL}$ concentration, suggesting that the AgNPs dissolve at a slower rate when dispersed at higher concentrations. In addition, the absorbance at 397 nm decreases more rapidly for smaller agglomerates compared to larger agglomerates. We hypothesize that this result reflects a greater release of silver ions from the less agglomerated particles due to their larger specific surface area.

Dependence of hemolysis on the agglomeration of AgNPs

To demonstrate the importance of controlling agglomeration in nanotoxicity studies, we chose to use the ASTM protocol 'E 2524 – 08: Standard Test Method for Analysis of Hemolytic Properties of Nanoparticles' to test hemolysis by AgNPs. This protocol works well for NPs that do not agglomerate in physiologic solutions, but it does not provide a mechanism for controlling the agglomeration of NPs apart from prescribing that the highest concentration of NPs to be used must be 'well dispersed in a physiologic solution'. Many NPs, such as the AuNPs and AgNPs used in this work, will agglomerate quickly in physiologic solutions except at extremely low concentrations unless a stabilizer such as protein is added. If protein is added to the initial dispersion, the protocol calls for dilution with phosphate buffered saline, so that the protein is diluted at the same time as the NPs. This dilution protocol would make it difficult to distinguish effects of diluting the NPs from diluting the protein (which is indicated by our preliminary results to be important for AgNPs since increasing BSA concentration decreases the hemolytic activity of AgNPs, results not shown). Therefore, for this work, we have modified the hemolysis protocol by dispersing the NPs in cell culture media, adding 2% BSA after a defined period of time, and then performing serial dilutions with DMEM + 2% BSA before adding blood. This altered protocol produces relatively stable dispersions of single particles or

agglomerates in physiologic solutions that are identical apart from the AgNP agglomeration state. This altered protocol expands the applications of the original hemolysis protocol to many more types of NPs and facilitates the reliable and reproducible study of the dependence of hemolysis on NP agglomeration.

Figure 7 shows that hemolysis decreases as the mean AgNP agglomerate size increases. Since Ag^+ ions are known to cause hemolysis (Sopjani et al. 2009) and AgNPs are known to release silver ions (Liu and Hurt 2010), the decreased hemolysis caused by larger AgNP agglomerates may be a result of the smaller effective specific surface area after agglomeration, resulting in less Ag^+ ion dissolution. The specific surface area of fractal-shaped agglomerates (Weitz and Oliveria 1984; Chithrani et al. 2006; Hotze et al. 2008; Hutter et al. 2010) is difficult to quantify, but it almost certainly decreases with increasing agglomeration. This hypothesis is supported by the slower decrease in absorbance at 390 nm of the larger agglomerates compared to the smaller agglomerates in Figure 4b.

Important parameters when dispersing nanoparticles

Agglomeration of NPs is likely to affect their toxicity in many ways, as described above. Therefore, creating reproducible dispersions of NPs is critical for performing reproducible nanotoxicity experiments. Achieving reproducible dispersions requires careful control of several parameters.

- (1) The timing between mixing steps and between the dispersion and toxicity experiments is frequently important. Many NPs will agglomerate quickly in media without proteins, which makes it difficult to study the toxicity without careful control of timing and careful interpretation of the results. Even for NPs dispersed in media with proteins, some NPs (e.g., silver) dissolve over time, so the timing between dispersion and toxicity experiments is likely to be important.
- (2) The concentrations of the NPs *both* in their initial solution and in the dispersed solution frequently affect agglomeration, even when the NPs are dispersed directly in media containing proteins. At higher concentrations, the NPs will often agglomerate slightly before they can be completely coated with protein (e.g., 110 $\mu\text{g/mL}$ AgNPs in Figure 4 and when starting with 10 mg/mL PS NPs in Figure 6). Even with the same dispersed concentration of PS NPs, the agglomerate size differed depending on whether

a 10 mg/mL or 1 mg/mL aqueous solution was pipetted into the media. Therefore, care should be taken when choosing how to perform the dilutions of NPs for toxicity experiments, since the chosen starting concentration frequently affects the agglomeration state.

- (3) Especially when dispersing high concentrations of NPs, the mixing rate of the media *while* the NP solution is being pipetted frequently affects agglomeration, probably because mixing disperses the NPs more quickly throughout the medium and increases transport of proteins to the NP surface. For example, AgNPs dispersed at 110 $\mu\text{g/mL}$ are smaller and more reproducible when vortexing at a higher speed, and polystyrene NPs agglomerate to a mean size of ~ 200 nm when mixed quickly compared to a mean size of up to 1600 nm without mixing. Therefore, if NPs are pipetted into a stagnant solution, the mean agglomerate size and its reproducibility should be measured.

Conclusions

We have demonstrated a reproducible method to create stable NP agglomerates of different sizes in an otherwise identical cell culture media by following the method illustrated in Figure 1. This method allows reproducible study of the agglomeration-dependence of hemolysis by AgNPs. The resulting protein-stabilized dispersions in physiological media are expected to be applicable to a wide variety of *in vitro* and *in vivo* nanotoxicity experiments, with additional possible applications in NP-based drug delivery and in cellular imaging due to the near-infrared absorption and surface-enhanced Raman scattering of agglomerates (Roca and Haes 2008). Here, we controlled the agglomeration of four types of metal, metal oxide, and polymer NPs, and we expect the protocol to be applicable to many types of NPs since many types have been shown to be stabilized by protein adsorption (Chithrani et al. 2006; Bihari et al. 2008; Murdock et al. 2008; Jiang et al. 2009; Kittler et al. 2010; MacCuspie et al. 2010; Tantra et al. 2010; Xie et al. 2010). By enabling the experimental determination of the dependence of toxicity exclusively on agglomeration size, this method is expected to improve structure-activity relationship models used to predict toxicity from NP characteristics (Alvarez et al. 2009). We also introduce modifications often important when using DLS to characterize the agglomerates, utilizing theory previously developed to account for rotation and vibration of the agglomerates as well as deriving new procedures to compensate for scattering due to BSA. Both of these modifications frequently affect the apparent diameter by a factor of

two or more. Because this method is 'bottom-up' (i.e., starting with single NPs), colloidal aggregation theory can be used to predict the approximate size distribution of agglomerates from the size measured by DLS. In contrast, when starting with agglomerates and breaking them apart by sonication, it is much more difficult to predict the size distribution theoretically. The agglomeration process described here is unlikely to damage the particles, break apart or form aggregates, or damage proteins. The mixing conditions of the NPs with physiologically-relevant media (e.g., mixing speed and NP concentration) and the timing between dispersing the NPs and measuring their toxicity are shown to be critical for achieving reproducible dispersions, sometimes affecting the size by a factor of 10. Therefore, it is important to consider these types of effects when performing toxicity studies or other biological assays with NPs. Finally, because a single NP solution is used to create all agglomerated solutions, this method permits the study of the dependence of toxicity exclusively on agglomerate size and shape while all other parameters are held constant (e.g., media composition and NP composition).

Declaration of interest: JMZ was funded by a National Research Council Postdoctoral Fellowship at NIST. MDH was supported in part by the National Science Foundation's Research Experience for Undergraduates (REU) program through the NIST Summer Undergraduate Research Fellowship (SURF) program. The authors report no conflict of interest. The authors alone are responsible for the content and writing of the paper.

References

- Alvarez PJJ, Colvin V, Lead J, Stone V. 2009. Research priorities to advance eco-responsible nanotechnology. *Acs Nano* 3(7): 1616–1619.
- Bihari P, Vippola M, Schultes S, Praetner M, Khandoga AG, Reichel CA, Coester C, Tuomi T, Rehberg M, Krombach F. 2008. Optimized dispersion of nanoparticles for biological in vitro and in vivo studies. *Particle and Fibre Toxicology* 5:14.
- Chithrani BD, Ghazani AA, Chan WCW. 2006. Determining the size and shape dependence of gold nanoparticle uptake into mammalian cells. *Nano Letters* 6(4):662–668.
- Duan JS, Park K, MacCuspie RI, Vaia RA, Pachter R. 2009. Optical properties of rodlike metallic nanostructures: Insight from theory and experiment. *J Phys Chem C* 113(35):15524–15532.
- Elghanian R, Storhoff JJ, Mucic RC, Letsinger RL, Mirkin CA. 1997. Selective colorimetric detection of polynucleotides based on the distance-dependent optical properties of gold nanoparticles. *Science* 277(5329):1078–1081.
- Greish K. 2007. Enhanced permeability and retention of macromolecular drugs in solid tumors: A royal gate for targeted anticancer nanomedicines. *J Drug Targeting* 15(7–8):457–464.
- Hotze EM, Bottero J-Y, Wiesner MR. 2010. Theoretical framework for nanoparticle reactivity as a function of aggregation state. *Langmuir* 26(13):11170–11175.

- Hotze EM, Labille J, Alvarez P, Wiesner MR. 2008. Mechanisms of photochemistry and reactive oxygen production by fullerene suspensions in water. *Environ Sci Technol* 42(11):4175–4180.
- Hussain SM, Braydich-Stolle LK, Schrand AM, Murdock RC, Yu KO, Mattie DM, Schlager JJ, Terrones M. 2009. Toxicity evaluation for safe use of nanomaterials: Recent achievements and technical challenges. *Adv Materials* 21(16):1549–1559.
- Hussain SM, Javorina AK, Schrand AM, Duhart HM, Ali SF, Schlager JJ. 2006. The interaction of manganese nanoparticles with PC-12 cells induces dopamine depletion. *Toxicological Sci* 92(2):456–463.
- Hutter E, Boridy S, Labrecque S, Lalancette-Hebert M, Kriz J, Winnik FM, Maysinger D. 2010. Microglial response to gold nanoparticles. *ACS Nano* 4(5):2595–2606.
- Jiang JK, Oberdorster G, Biswas P. 2009. Characterization of size, surface charge, and agglomeration state of nanoparticle dispersions for toxicological studies. *J Nanopart Res* 11(1):77–89.
- Kato H, Fujita K, Horie M, Suzuki M, Nakamura A, Endoh S, Yoshida Y, Iwahashi H, Takahashi K, Kinugasa S. 2010. Dispersion characteristics of various metal oxide secondary nanoparticles in culture medium for in vitro toxicology assessment. *Toxicol in Vitro* 24(3):1009–1018.
- Kim KT, Klaine SJ, Cho J, Kim SH, Kim SD. 2010a. Oxidative stress responses of *Daphnia magna* exposed to TiO₂ nanoparticles according to size fraction. *Sci Total Environ* 408(10):2268–2272.
- Kim SC, Chen DR, Qi CL, Gelein RM, Finkelstein JN, Elder A, Bentley K, Oberdörster G, Pui DYH. 2010b. A nanoparticle dispersion method for in vitro and in vivo nanotoxicity study. *Nanotoxicology* 4(1):42–51.
- Kittler S, Greulich C, Gebauer JS, Diendorf J, Treuel L, Ruiz L, Gonzalez-Calbet JM, Vallet-Regi M, Zellner R, Koller M, et al. 2010. The influence of proteins on the dispersability and cell-biological activity of silver nanoparticles. *J Materials Chem* 20(3):512–518.
- Limbach LK, Grass RN, Stark WJ. 2009. Physico-chemical differences between particle- and molecule-derived toxicity: Can we make inherently safe nanoparticles? *Chimia* 63(1–2):38–43.
- Limbach LK, Wick P, Manser P, Grass RN, Bruinink A, Stark WJ. 2007. Exposure of engineered nanoparticles to human lung epithelial cells: Influence of chemical composition and catalytic activity on oxidative stress. *Environ Sci Technol* 41(11):4158–4163.
- Lin MY, Lindsay HM, Weitz DA, Klein R, Ball RC, Meakin P. 1990. Universal diffusion-limited colloid aggregation. *J Phys-Condensed Matter* 2(13):3093–3113.
- Link S, Mohamed MB, El-Sayed MA. 1999. Simulation of the optical absorption spectra of gold nanorods as a function of their aspect ratio and the effect of the medium dielectric constant. *J Phys Chem B* 103(16):3073–3077.
- Liu JY, Hurt RH. 2010. Ion release kinetics and particle persistence in aqueous nano-silver colloids. *Environ Sci Technol* 44(6):2169–2175.
- Lundqvist M, Stigler J, Elia G, Lynch I, Cedervall T, Dawson KA. 2008. Nanoparticle size and surface properties determine the protein corona with possible implications for biological impacts. *Proceedings of the National Academy of Sciences of the USA* 105(38):14265–14270.
- MacCuspie RI, Allen AJ, Hackley VA. 2010. Dispersion stabilization of silver nanoparticles in synthetic lung fluid studied under in situ conditions. *Nanotoxicology* published online (DOI: 10.3109/17435390.2010.504311).
- Murdock RC, Braydich-Stolle L, Schrand AM, Schlager JJ, Hussain SM. 2008. Characterization of nanomaterial dispersion in solution prior to In vitro exposure using dynamic light scattering technique. *Toxicol Sci* 101(2):239–253.
- Okuda-Shimazaki J, Takaku S, Kanehira K, Sonezaki S, Taniguchi A. 2010. Effects of titanium dioxide nanoparticle aggregate size on gene expression. *Int J Mol Sci* 11:2383–2392.
- Park EJ, Yi J, Chung YH, Ryu DY, Choi J, Park K. 2008. Oxidative stress and apoptosis induced by titanium dioxide nanoparticles in cultured BEAS-2B cells. *Toxicol Lett* 180(3):222–229.
- Park EJ, Yi J, Kim Y, Choi K, Park K. 2010. Silver nanoparticles induce cytotoxicity by a Trojan-horse type mechanism. *Toxicol in Vitro* 24(3):872–878.
- Roca M, Haes AJ. 2008. Probing cells with noble metal nanoparticle aggregates. *Nanomedicine* 3(4):555–565.
- Sager TM, Porter DW, Robinson VA, Lindsley WG, Schwegler-Berry DE, Castranova V. 2007. Improved method to disperse nanoparticles for in vitro and in vivo investigation of toxicity. *Nanotoxicology* 1(2):118–129.
- Schrand AM, Huang HJ, Carlson C, Schlager JJ, Osawa E, Hussain SM, Dai LM. 2007. Are diamond nanoparticles cytotoxic? *J Phys Chem B* 111(1):2–7.
- Sharma VK. 2009. Aggregation and toxicity of titanium dioxide nanoparticles in aquatic environment-A Review. *J Environ Sci Health Part a – Toxic/Hazardous Substances Environ Engineer* 44(14):1485–1495.
- Sopjani M, Foller M, Haendeler J, Gotz F, Lang F. 2009. Silver ion-induced suicidal erythrocyte death. *J Appl Toxicol* 29(6):531–536.
- Tantra R, Tompkins J, Quincey P. 2010. Characterisation of the de-agglomeration effects of bovine serum albumin nanoparticles in aqueous suspension. *Coll Surf B* 75:275–281.
- Taurozzi JT, Hackley VA, Wiesner MR. 2010a. Ultrasonic Dispersion of Nanoparticles for Environmental, Health and Safety Assessment – Issues and Recommendations. *Nanotoxicology*. published online (DOI: 10.3109/17435390.2010.528846).
- Taurozzi JT, Hackley VA, Wiesner MR. 2010b. Preparation of nanoparticle dispersions from powdered material using ultrasonic disruption. *CEINT-NIST Protocol* 1:1–10.
- Taurozzi JT, Hackley VA, Wiesner MR. 2010c. Reporting guidelines for the preparation of aqueous nanoparticle dispersions from dry nanomaterials. *CEINT-NIST Protocol* 2:1–5.
- Usenko CY, Harper SL, Tanguay RL. 2008. Fullerene C-60 exposure elicits an oxidative stress response in embryonic zebrafish. *Toxicol Appl Pharmacol* 229(1):44–55.
- Weitz DA, Oliveria M. 1984. Fractal structures formed by kinetic aggregation of aqueous gold colloids. *Phys Rev Lett* 52(16):1433–1436.
- Wiesner MR, Lowry GV, Jones KL, Hochella MF, Di Giulio RT, Casman E, Bernhardt ES. 2009. Decreasing uncertainties in assessing environmental exposure, risk, and ecological implications of nanomaterials. *Environ Sci Technol* 43(17):6458–6462.
- Xie J, Wang JH, Niu G, Huang J, Chen K, Li XG, Chen XY. 2010. Human serum albumin coated iron oxide nanoparticles for efficient cell labeling. *Chem Commun* 46(3):433–435.

Supplementary material available online

Several standards organizations' definitions of aggregate and agglomerate, absorbance spectra at additional time points, and AFM images.